UC Berkeley
UC Berkeley Previously Published Works

Title

Erratum: "Electron attachment dynamics following UV excitation of iodide-2-thiouracil complexes" [J. Chem. Phys. 156, 244302 (2022)]

Permalink

Journal

ISSN

Authors

Koga, Masafumi
Asplund, Megan
Neumark, Daniel M

Publication Date

2022-07-28

DOI

Peer reviewed

Electron attachment dynamics following UV excitation of iodide-2-thiouracil complexes

Masafumi Koga, Megan Asplund and Daniel M. Neumark

View Online   Export Citation   CrossMark

ARTICLES YOU MAY BE INTERESTED IN

Electron attachment dynamics following UV excitation of iodide-2-thiouracil complexes

Masafumi Koga,[1] (iD) Megan Asplund,[1] and Daniel M. Neumark[1,2,a] (iD)

AFFILIATIONS

[1] Department of Chemistry, University of California, Berkeley, California 94720, USA
[2] Chemical Sciences Division, Lawrence Berkeley National Laboratory, Berkeley, California 94720, USA

[a] Author to whom correspondence should be addressed: dneumark@berkeley.edu

ABSTRACT

The dynamics of low energy electron attachment to the thio-substituted uracil analog 2-thiouracil are investigated using time-resolved photoelectron spectroscopy (TRPES) of iodide-2-thiouracil ($I^-\cdot 2TU$) binary clusters. In these experiments, the anions are excited at pump energies of 4.16 and 4.73 eV, and the ensuing dynamics are probed by photodetachment at 1.59 and 3.18 eV. Upon excitation near the vertical detachment energy (4.16 eV), dipole bound (DB) and valence bound (VB) anion signals appear almost instantaneously, and the DB state of the 2TU anion undergoes an ultrafast decay (~50 fs). At 4.73 eV, there is no evidence for a DB state, but features attributed to two VB states are seen. The transient negative ions formed by photoexcitation decay by autodetachment and I^- fragmentation. The I^- dissociation rates and their dependence on excitation energy agree reasonably well with the Rice–Ramsperger–Kassel–Marcus calculations. Notable differences with respect to TRPES of the related iodide–uracil anion are observed and discussed.

Published under an exclusive license by AIP Publishing. https://doi.org/10.1063/5.0098280

I. INTRODUCTION

The role of radiation in causing DNA strand cleavage has long been known, and in the past few decades, it has become clear that indirect interactions via low-energy electrons (LEEs) contribute significantly to this process.[1] During electron capture, an excess electron can occupy an unoccupied valence orbital of a nucleobase to form a valence-bound (VB) anionic state, but it can also be captured by a sufficiently large dipole moment on the base to form a diffuse dipole-bound (DB) state.[2] This DB state is proposed to serve as a "doorway" to electron capture.[3,4] However, since the interaction of LEEs with nucleobases is diffusion-controlled in the condensed phase, the primary processes of electron attachment at the moment of electron capture have been difficult to characterize.

To elucidate the dynamics of electron capture by nucleobases in the gas phase, we have previously studied the photoinduced dynamics of iodide–nucleobase cluster anions[5] $I^-\cdot$thymine,[6–8] $I^-\cdot$adenine,[9] $I^-\cdot$uracil,[6,8,10,11] and $I^-\cdot$uracil H_2O[12,13] by means of femtosecond time-resolved photoelectron spectroscopy (TRPES).[14] In these experiments, an ultraviolet pump pulse photoexcites the complex, triggering electron transfer from the iodide to the nucleobase and forming a transient negative ion (TNI) whose dynamics can be probed by a second laser pulse that induces photodetachment. Complementary experiments on the photodepletion of several of these species have been carried out by Dessent and co-workers.[15–17]

The nature and dynamics of the TNI depend on the energy of the excitation pulse. In the $I^-\cdot$uracil ($I^-\cdot U$) cluster, which is one of the more intensively investigated systems, excitation near the vertical detachment energy (VDE) gives rise to both DB and VB states immediately after photoexcitation. The appearance timescales of these TNIs suggest partial DB → VB conversion on a timescale of ~200 fs. The partial conversion reflects the fact that in uracil, the DB anion is slightly lower in energy than the VB anion.[18,19] Moreover, different dynamics are observed when $I^-\cdot U$ is excited around 4.7 eV, which is well above the cluster VDE. In this case, the VB state is generated immediately, and there is no evidence for the formation of the DB state.[11,13] Quantum chemical calculations suggest that the oscillator strength for optical charge transfer of the excess electron of I^- to the vacant π^* orbital of the nucleobase is negligibly small at this excitation energy; it was thus proposed that ultrafast population of the VB state of the nucleobase arises $\pi\pi^*$ excitation of the nucleobase followed by charge transfer from I^-.[11] A global discussion of the excitation and decay mechanisms of iodide–nucleobase
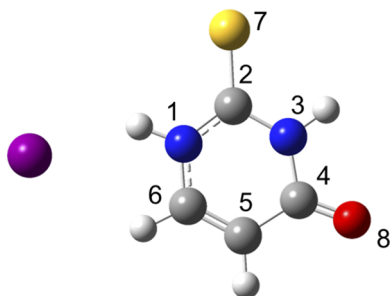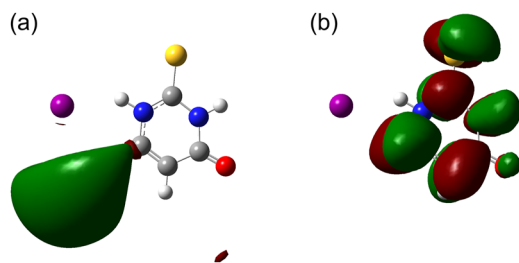
FIG. 1. Ground-state structure of the iodide-2TU cluster obtained at the MP2/aug-cc-pVDZ(-pp) level of theory. Atom numbering of 2TU is also shown.

TABLE I. Adiabatic electron affinity (AEA) and vertical electron affinity (VEA) of U and 2TU anions (in meV).

Species	DB state	VB state	
	AEA	AEA	VEA
U[a]	93	40	−572
2TU[b]	⋯	174	−173

[a]References 18 and 19.
[b]Reference 29.

complexes was presented by Kunin and Neumark,[5] but several open questions remain.

In this study, we carry out TRPES experiments on the I⁻·2TU cluster (Fig. 1), replacing uracil with 2-thiouracil (2TU) in which the oxygen bonded to carbon C2 is substituted with sulfur. Thiosubstituted nucleobases play essential roles in medical applications, especially in light and radiation chemotherapy, so understanding electron capture dynamics of these species is desirable.[20–23] Dessent[24] investigated the one-photon photodepletion and photofragmentation spectra of I⁻·2TU and found that it exhibits two pronounced features: a distinct peak at 4.1 eV and a rather flat region above 4.6 eV. The peak at 4.1 eV was assigned to a charge transfer transition from iodide to a diffuse DB orbital of 2TU [Fig. 2(a)], as had been seen in I⁻·U. Excitation at >4.6 eV was attributed to a combination of direct detachment and a $\pi\pi^*$ transition localized on the thiouracil, an assignment consistent with the electronic spectroscopy of this species.[25] Other relevant experiments include measurements of dissociative electron attachment to 2TU[26,27] and anion photoelectron spectroscopy of the related species 4TU⁻ and 2,4TU⁻.[28]

Ortiz and co-workers[29] carried out electronic structure calculations on 2TU⁻, obtaining results for the adiabatic electron affinity (AEA) and vertical electron affinity (VEA) for 2TU and the vertical detachment energy (VDE) of the anion; these values are 0.26, −0.17, and 0.71 eV, respectively. These numbers apply to the VB state of 2TU⁻ in which the lowest π^* orbital [Fig. 2(b)] is occupied, although a DB state is also expected owing to the high dipole moment of 2TU (4.20 D). Since the diffuse electron in a DB state is typically bound by 0.1 eV or less, the calculations suggest that, in contrast to the uracil

FIG. 2. Schematics of singly occupied orbitals of the (a) DB state and (b) VB state of the 2TU anion in I⁻·2TU.

anion (see Table I), the VB state of 2TU⁻ lies below its DB state. As a result, the dynamics of DB to VB conversion in photoexcited I⁻·2TU might be expected to differ from those seen in I⁻·U, motivating, in part, the work presented here.

The TRPES experiments on I⁻·2TU described herein are carried out at two pump energies: 4.16 eV, near the VDE of the cluster, and 4.73 eV, which is in the range of one or more $\pi\pi^*$ transitions on the 2TU chromophore. As in previous studies, a 1.59 eV pulse is used as a probe for the observation of DB and VB state dynamics, and a 3.18 eV probe pulse is used for monitoring other transient species and products related to the deactivation of VBS. In particular, the 3.18 eV probe pulse enables electron photodetachment of dissociated iodide, which has an eBE of 3.06 eV, and is expected to be one of the major products following UV irradiation.

Our experiments reveal rapid formation of DB and VB anions upon near VDE excitation. The DB state undergoes nearly complete ultrafast (<100 fs) conversion to the VB state, and the resulting VB signal decays in ~10 ps. Excitation at 4.73 eV gives rise to the VB state and a higher-lying π^* state that also plays a role in the TNI dynamics. Following excitation with either pump energy, the I⁻ signal grows in within ~10 ps, which is notably faster than for other I⁻ nucleobases we have studied[11,13] and, in fact, agrees with the calculated time scale for statistical dissociation of energized I⁻·2TU. This agreement indicates that dissociation to I⁻ proceeds without the dynamic bottlenecks seen in previous systems.

II. METHODS

A. Experimental

The TRPES setup has been described in detail elsewhere.[14,30,31] Briefly, iodide-2-thiouracil clusters are formed by flowing 300 kPa of argon over a reservoir containing iodomethane and through a cartridge containing the solid 2-thiouracil sample (Aldrich >97%). This cartridge is housed within an Even–Lavie pulsed valve operating at 500 Hz and heated to 220 °C to achieve volatilization. The pulsed valve produces a supersonic expansion of the gas mixture into vacuum that passes through a ring ionizer, generating charged species by secondary electron attachment. Ions are then extracted perpendicularly into a Wiley–McLaren mass spectrometer,[32] and iodide-2-thiouracil ion clusters are mass-selected for subsequent interaction with laser pulses.

TRPES employs a pump–probe scheme of femtosecond laser pulses to first excite the ion clusters and then photodetach electrons for detection. A laser system comprising a KM Griffin oscillator and

Dragon amplifier operating at 1 kHz generates ~40 fs laser pulses centered at 780 nm (1.59 eV) with a 2 mJ/pulse. To generate a pump pulse at 4.16 eV, a portion of this output is sent to a TOPAS-C optical parametric amplifier (OPA), which generates 596-nm light that is subsequently doubled in a beta-barium borate (BBO) crystal to form an excitation pulse at 298 nm (4.16 eV). Pump pulses at 4.73 eV are generated by frequency-tripling the 780 nm pulse. Two probing schemes are also employed: one using the fundamental of the output from the KM amplifier (1.59 eV) and the second utilizing a frequency doubled pulse at 390 nm (3.18 eV).

Detached electrons are detected using a chevron mounted pair multi-channel plates coupled to a phosphor screen and imaged using a charge-coupled device (CCD) camera. The basis set expansion (BASEX) method was used to reconstruct the kinetic energies of the imaged photoelectrons.[33]

B. Computational

The Gaussian 16 computing package[34] was used to generate the potential energy surface for the dissociation of $I^-·2TU$ to $I^- + 2TU$ at the MP2 level with an augmented Dunning basis set (aug-cc-pVDZ) for C, H, O, and N and an additional set of diffuse functions (aug-cc-pVDZ-pp) for I.[35] Geometry optimization and vibrational frequency calculations were performed as a function of I–N1 distance, with steps of 0.25 Å far from the transition state and 0.1 Å within 1 Å of the transition state. The resulting potential energy curve and geometries at several characteristic points are shown in the supplementary material.

III. RESULTS

Figure 3 shows one-photon photoelectron spectra of the $I^-·2TU$ binary complex recorded at photon energies of 4.16 and 4.73 eV. The spectrum taken at 4.73 eV has two prominent features. The peak at an electron kinetic energy (eKE) of ~0.62 eV arises from direct detachment to the $^2P_{3/2}$ spin–orbit state of complexed iodine and yields a vertical detachment energy (VDE) of 4.11 eV (i.e., 4.73–0.62 eV) for the cluster. From this, we can determine that solvation by 2TU stabilizes the I^- anion by about 1 eV, given that EA(I) = 3.06 eV. This solvent shift is similar to that found for the $I^-·U$ complex.[8] The width of this peak is ~0.2 eV and is broader than that of
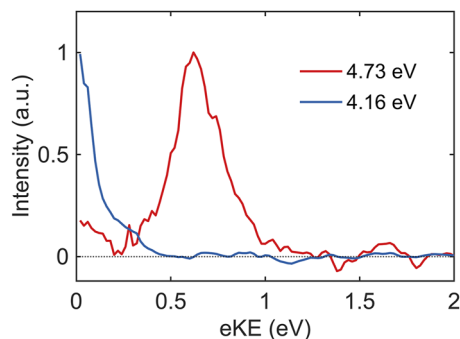
$I^-·U$ (~0.1 eV) at the corresponding excitation energy.[11] This suggests a greater geometric displacement of the $I^-·2TU$ complex from the corresponding neutral species than for $I^-·U$. The second, smaller feature of the photoelectron spectrum occurs at nearly zero kinetic energy and is attributed to autodetachment from the transient negative ion, which is known to produce low energy electrons from these systems.[11–13,36] The spectrum shows that direct detachment dominates at 4.73 eV, consistent with the results of Dessent.[24]

At 4.16 eV, which lies just 50 meV above the VDE, only the ~0 eV feature is seen. Although it is tempting to ascribe all signal intensity to autodetachment, direct cluster detachment also leads to low kinetic energy electrons, so one cannot readily distinguish between electrons produced by the two mechanisms.

A. TRPES with the 1.59-eV probe

Figure 4 shows a contour plot of the TRPE spectrum of $I^-·2TU$ excited at 4.16 eV and detached with a 1.59 eV probe pulse. According to Dessent,[24] excitation at this energy accesses a DB state of the anion. This spectrum is plotted as a function of electron binding energy (eBE = $h\nu$ – eKE). In Fig. 4, two distinctive features appear immediately following excitation: a sharp peak centered at around 0.1 eV (feature A) and a broad signal with an intensity maximum at ~0.7 eV (feature B). Based on its low binding energy and narrow width, feature A is assigned to a DB transient negative ion.[10] Feature B, with a higher eBE and greater spectral breadth, is then attributed to a VB transient negative ion. These assignments are in agreement with previous investigations of iodide–nucleobase complexes[5] and with the theoretically predicted VDE of the VB canonical anion (0.71 eV).[29] Feature A decays within ~100 fs, losing its characteristic narrow shape. The broad feature B also appears rapidly following excitation, before decaying within several picoseconds. The analysis in Sec. IV suggests that the persistent residual signal in the energy range of feature A is from the low energy tail of feature B.

Figure 5 shows the TRPE spectrum excited at 4.73 eV and probed at 1.59 eV. Any signal with eBE >0.85 eV is excluded from Fig. 5 because of large intensity fluctuations in the direct detachment signal caused by the pump pulse. In contrast to Fig. 4, there

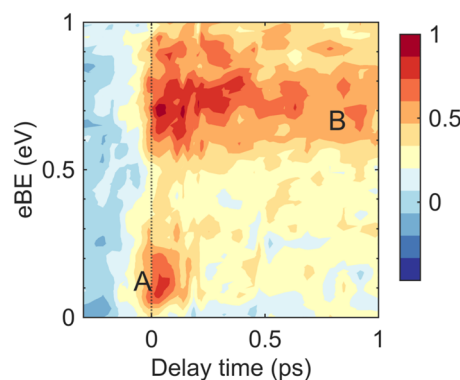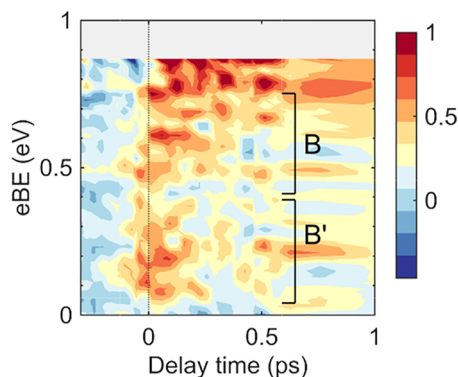**FIG. 3.** One photon photoelectron spectra of $I^-·2TU$ with the photon energies of 4.73 eV (red) and 4.16 eV (blue).

FIG. 4. Contour plot of TRPE spectra of $I^-·2TU$ with excitation and probe pulses of 4.16 eV and 1.59 eV, respectively.

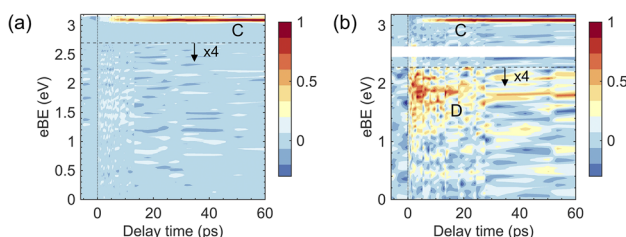**FIG. 5.** Contour plot of TRPE spectra of I⁻·2TU at excitation and probe energies of 4.73 eV and 1.59 eV.

is no sharp, strong feature at around 0 eV. Instead, a broad feature is seen rapidly following photoexcitation, with the greatest intensity from 0.6 to 0.8 eV, a range very similar to that of the VB state observed with 4.16 eV excitation. This result strongly indicates that the DB state does not form at 4.73 eV but that the VB state is populated shortly after excitation, giving rise to the strong signal at around 0.7 eV (feature B). A second, relatively strong photoelectron feature is observable at 0–0.45 eV, especially at early time scales (feature B′).

B. TRPES with the 3.18-eV probe

Figures 6(a) and 6(b) show TRPE spectra probed at 3.18 eV. In each plot, the most prominent feature, feature C, is located at 3.06 eV and grows in intensity over tens of ps. Based on its binding energy and spectral shape, this feature is clearly from photodetachment of atomic iodide produced by photofragmentation of I⁻·2TU. In addition, Fig. 6(b) exhibits a broad and very weak feature D at 1.3–2.2 eV, which appears within 1 ps and then slowly decays within ~10 ps, leaving a small offset component at 60 ps. This feature is negligibly small in Fig. 6(a).

IV. ANALYSIS

To gain a more quantitative understanding of our results, the signal intensity of each feature in Figs. 4–6 is integrated over a

FIG. 6. Contour plots of TRPE spectra of I⁻·2TU photodetached by 3.18 eV with excitation energies of (a) 4.16 eV and (b) 4.73 eV. The signal intensities below 2.7 eV in (a) and 2.28 eV in (b) are magnified by a factor of 4.

TABLE II. Fit parameters that reproduce the time evolution in Fig. 7.

	eBE (eV)	τ_1 (fs)	τ_2 (ps)	A_1	A_2
Feature A	0–0.20	55 ± 25	10.6 ± 4.4	0.89[a]	0.11
Feature B	0.5–1.0	260 ± 90	9.6 ± 1.5	0.46	0.54

[a]All amplitudes shown here are normalized by the sum of the decay amplitudes.

TABLE III. Time constants necessary to reproduce the time evolution in Fig. 8.

|	eBE (eV)	τ_1 (fs)	τ_2 (ps)	A_1	A_2
Feature B′	0–0.4	70 ± 20	35.6 ± 15.5	0.84[a]	0.16
Feature B	0.4–0.75	125 ± 65	52.8 ± 19.5	0.58	0.42

[a]All amplitudes shown here are normalized by the sum of the decay amplitudes.

specified eBE range (see Tables II and III) for each pump–probe delay. The results for pump energies of 4.16 and 4.73 eV are shown in Figs. 7 and 8, respectively, for a probe energy of 1.59 eV. As in previous work, these time-dependent integrated distributions are fit to the convolution of a Gaussian experimental response function with a sum of exponential functions using the following equation:

$$I(t) = \frac{1}{\sigma_{CC}\sqrt{2\pi}} \exp\left(-\frac{t^2}{2\sigma_{CC}^2}\right) \cdot \begin{cases} I_0, & t < 0, \\ I_0 + \sum_i A_i \exp\left(\frac{-t}{\tau_i}\right), & t \ge 0, \end{cases}$$

(1)

where I_0 represents a constant offset and the dot indicates convolution over time. σ_{CC} is the Gaussian cross correlation width of pump and probe pulses, determined to be 72 fs for 4.16 eV excitation and 70 fs for 4.73 eV. The free parameters of the fit are A_i and τ_i, the amplitudes and the time constants of the decays, respectively.

The integrated signals and fits for the data in Fig. 4 are shown in Fig. 7, and the fit parameters are shown in Table II. With these values, Eq. (1) accurately reproduces the time evolution of both features. The rise times of features A and B lie within the instrumental response function, and both features, then, undergo a bi-exponential decay. Most of feature A decays with a time constant of 55 fs. The faster decay of feature B is slower than this (260 fs), while the slower time constants for the two features are both around 10 ps, and there
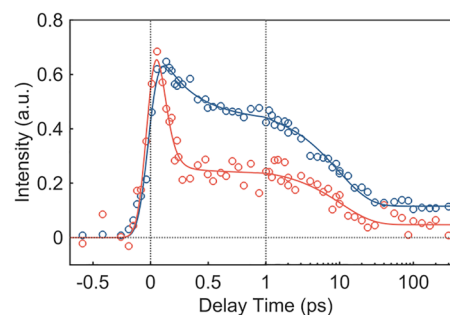
FIG. 7. Time evolution of the photoelectron intensity of feature A (red) and feature B (blue) as open circles. The time axis is linear up to 1 ps and logarithmic afterward. The results of the convolution fittings are also displayed as solid lines.
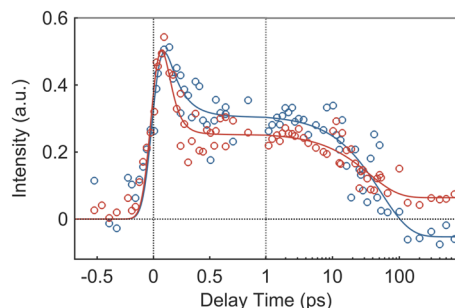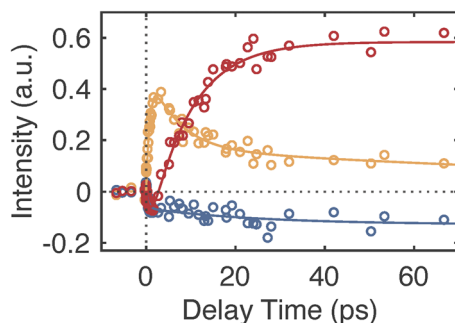
FIG. 8. Time evolution of integrated signal intensities of features B (blue) and B′ (red) in the TRPE spectra with 4.73 eV excitation.

is a nonzero offset that extends beyond 400 ps. A preliminary interpretation of these results, discussed in more detail in Sec. V, is that the DB state (feature A) decays to the VB state on a 55 fs time scale, and much of the VB state subsequently decays within 10 ps. The VB feature is quite broad and probably extends into the energy range of feature A, which is why both features exhibit the same 10 ps decay.

At 4.73 eV excitation, the broad signal in Fig. 5 is divided into two regions, 0.4–0.75 eV (feature B) and 0–0.4 eV (feature B′). The breadth and binding energy of both features suggest that they correspond to VB anion states. Their time evolution, together with the curve fitting results by Eq. (1), is plotted in Fig. 8, and the time constants required to reproduce the data are displayed in Table III.

Both features exhibit rise times within the IRF followed by biexponential decay. The fast decay constants for features B and B′ are 125 and 70 fs, respectively, lying between the values of the faster time constants for features A and B in Table II. On the other hand, the slower time constants of 53 and 36 ps for B and B′, respectively, are considerably larger than the 10 ps long-time decays for features A and B at 4.16 eV excitation. The decay channels responsible for these dynamics are discussed in Sec. V.

Additional insight into the decay dynamics is provided by the 3.18 eV probe. Figure 9 shows the time evolution of feature C at both pump energies and feature D with 4.73 eV excitation. The timescales

TABLE IV. Timescales describing features C (3.03–3.09 eV) and D (1.40–2.30 eV) for different excitation energies.

$h\nu$ (eV)	Feature	τ_1 (ps)	τ_2 (ps)	τ_3 (ps)	A_1	A_2	A_3
4.16	C	$\cdots$	13.9 ± 1.6	$\cdots$		-1.0^{a}	
4.74	C	0.98 ± 0.5	9.0 ± 1.2	$\cdots$	0.40^{a}	-1.4	
	D	0.84 ± 0.27	6.6 ± 3.4	180 ± 85	-0.105	0.065	0.040

[a] All amplitudes at each excitation energy are normalized by the offset values (I_{off}) of feature C at a long time delay.

of these curves are analyzed with a sum of exponential functions, as shown in the following equation:

$$I(t) = \begin{cases} 0, & t < 0, \\ I_{off} + \sum_i A_i \exp\left(\dfrac{-t}{\tau_i}\right), & t \geq 0, \end{cases} \qquad (2)$$
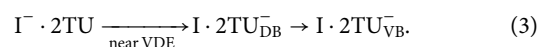
where I_{off} is the offset at long delay time. The resultant time constants are summarized in Table IV. At 4.16 eV, feature C shows a gradual rise, which is reproduced by the single-exponential function with a time constant of 13.9 ps, whereas at 4.73 eV, it exhibits depletion in the sub-picosecond timescale before the appearance of the positive signal with a rise time of 9 ps. Feature D at 4.73 eV exhibits a sub-picosecond rise and subsequent double-exponential decay with time constants of 6.6 and 180 ps.
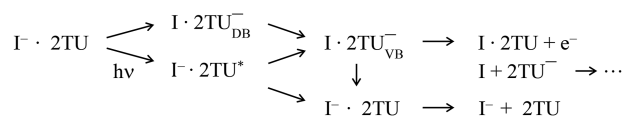
V. DISCUSSION

In this section, we discuss the excitation and decay processes responsible for the observed dynamics in I⁻·2TU. From our previous work on iodide-nucleobases, particularly I⁻·U, several pathways and channels are expected to be energetically accessible, as summarized in Scheme 1.[5] This array of possible channels provides the context for the remainder of the discussion in this section.

A. Excitation at 4.16 eV

According to Dessent,[24] excitation near the VDE results in transfer of an electron from the iodide to a DB state of 2TU, according to the following equation:

$$\text{I}^- \cdot 2\text{TU} \xrightarrow[\text{near VDE}]{} \text{I} \cdot 2\text{TU}_{\text{DB}}^- \rightarrow \text{I} \cdot 2\text{TU}_{\text{VB}}^-. \qquad (3)$$

This is consistent with the presence of feature A in Fig. 4 just after excitation. The DB state exhibits a rapid decay of 55 fs, and the most plausible explanation for this decay is conversion to the

FIG. 9. Time evolution of feature C (3.03–3.09 eV) with 4.16-eV excitation (blue) and that with 4.73-eV excitation (red) and feature D (1.40–2.30 eV, orange) with 4.73-eV excitation. The intensity of feature D is magnified by a factor of 4.
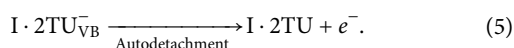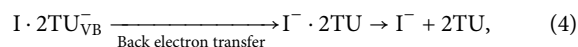

**SCHEME 1.** Overall decay channels of photoexcited I-•2TU cluster.

lowest VB state of 2TU$^-$. From this assignment, one might expect to see a corresponding delayed onset for the VB state. However, feature B appears almost simultaneously with feature A. Nonetheless, within the IRF, even if we analyzed the time evolution of the VB state with a triple-exponential function based on the assumption that there is also an ~50-fs rise component, the fitting curve is almost identical to that with a double-exponential function (see the supplementary material). Therefore, it is reasonable to assign the 55 fs decay to DB → VB conversion.

The calculated electron affinity to form the VB anion,[29] 0.174 eV, places it ~0.1 eV below the DB state (Fig. 10), enabling facile DB → VB conversion. Our assignment of the spectral features suggests that this conversion is essentially complete within 55 fs. This situation differs from I$^-$·U, in which DB → VB conversion occurs rapidly but the DB signal persists for many ps, indicating only partial conversion to the VB state,[5,10] a consequence of the DB state of U$^-$ lying below the VB state.[18] As another point of reference, the 55 fs decay is shorter than the DB → VB conversion time of 400 fs seen in I$^-$·CH$_3$NO$_2$, which has the same relative ordering of DB and VB states as I$^-$·2TU and demonstrates a near complete interconversion of the TNIs.[37]

Once the VB state is populated, it undergoes a bi-exponential decay with time constants of 260 fs and 9.6 ps, with a residual constant signal seen at >100 ps. The main deactivation pathways for this state are represented as follows:

$$I \cdot 2TU^-_{VB} \xrightarrow[\text{Back electron transfer}]{} I^- \cdot 2TU \rightarrow I^- + 2TU, \qquad (4)$$

$$I \cdot 2TU^-_{VB} \xrightarrow[\text{Autodetachment}]{} I \cdot 2TU + e^-. \qquad (5)$$

As reported by photofragment mass spectroscopy[24] and observed here in Fig. 6, iodide is the main dissociative photoproduct [Eq. (4)], which strongly indicates that back electron transfer to the I atom takes place as a primary deactivation channel of the VB state. In addition, autodetachment is expected as a decay channel of the VB anion, given that the excitation energy is ~50 meV higher than the VDE of the cluster (4.11 eV). I·2TU$^-_{VB}$ can dissociate to I + 2TU$^-$, and this fragment anion may be responsible for the long-lived signal seen in Fig. 7 since its photoelectron spectrum is expected to be very similar to that of I·2TU$^-_{VB}$. However, 2TU$^-$ was not observed in the photofragment mass spectrum measured by Dessent, so it may be formed here only as a long-lived transient
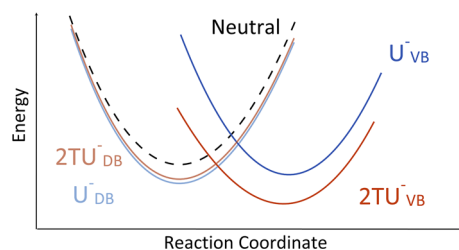

FIG. 10. Schematic diagram of the energy levels of the dipole bound anion and valence bound anion for 2TU (red) and U (blue) relative to those for the neutral species.

species. Previous mass spectroscopy has also detected the H-atom loss from the 2TU anion as a minor channel,[24] but the deprotonated anion cannot be detected in this experiment due to its large VDE (3.82 eV).[38]

The experiments at 3.18 eV probe energy clearly show that fragmentation to I$^-$ [feature C in Fig. 6(a)] occurs with a rise time of ~14 ps. To elucidate the I$^-$ dissociation kinetics in detail, we calculated the dissociation rate based on the Rice–Ramsperger–Kassel–Marcus (RRKM) model.[39,40] In this calculation, energies and frequencies obtained by MP2 calculations were used to determine the density of states by the Beyer–Swinehart direct count algorithm with the Stein–Rabinovitch modification.[41,42] The in-plane rocking mode and out-of-plane twisting mode are treated as hindered rotors because their frequencies decrease notably as the N1–I length increases. Further description of this calculation is found in the supplementary material. We calculate a dissociation rate constant of 4.80×10^{10} s^{-1} (20.8 ps), which is in reasonable agreement with the experimental value. Assuming that the 260 fs decay constant of feature B includes back-electron transfer, this process would re-form I$^-$·2TU with sufficient vibrational energy to fragment to I$^-$, so agreement with the RRKM result is not surprising. On the other hand, this result differs notably from I$^-$·U where the time constant for I$^-$ production is much longer than the RRKM prediction; possible reasons are discussed in Sec. V C.

B. Excitation at 4.73 eV

When I$^-$·2TU is excited at 4.73 eV, the VB state signal appears within the cross correlation of the laser, while DB signal is notably absent. This matches the results observed for I$^-$·U at a similar excitation energy.[8,10] Various mechanisms have been proposed for the near instantaneous production of the VB state in I$^-$·U,[10,11] but the most plausible is that it arises via localized $\pi\pi^*$ excitation of uracil followed by ultrafast excess electron transfer from iodide into the hole created by this excitation, as given in the following equation:

$$I^- \cdot 2TU \xrightarrow[\pi\pi^*]{} I^- \cdot 2TU^* \rightarrow I \cdot 2TU^-_{VB}. \qquad (6)$$
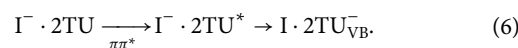
In I$^-$·2TU, two broad bands (features B and B$'$) appear within the IRF and decay bi-exponentially. The faster decay time constants are 125 fs for feature B and 70 fs for feature B$'$. Although these time constants are within error, the distinct additional feature B$'$ and its faster decay rate suggest that two VB states are present. This interpretation is consistent with the UV spectrum of 2-thiouracil,[43] in which excitation at 4.73 eV can access two overlapped excited states comprising the $\pi_s\pi_6^*$ and, at higher energy, the $\pi_s\pi_2^*$ transitions, with the π^* orbitals localized around C6 and C2, respectively (see Fig. 1). Hence, the mechanism in Eq. (6) can initially result in two VB anion states corresponding to the excess electron residing in either the π_6^* or π_2^* orbitals, leading to feature B or B$'$ in the TRPE spectrum. The 70 fs decay constant for B$'$ can represent a combination of internal conversion to the lower VB state, autodetachment, and back-electron transfer to the I atom. The 125 fs decay time for the lower VB state is attributed to the latter two processes.

The rise of the iodide peak (feature C)st this 4.73 eV pump energy is significantly faster (9 ps) than that at 4.16 eV (14 ps). This value is again in reasonable agreement with the rate calculated with RRKM theory calculations predict that I$^-$ should appear in 11.8 ps. Hence, the excited states of I$^-$·2TU decay to the ground state

rapidly enough for iodide to dissociate with timescales statistically determined by the excitation energies.

At this higher excitation energy, re-formation of the ground state with sufficient vibrational energy for I^- dissociation is possible not only by back electron transfer but also via internal conversion from excited states localized on the chromophore, as was seen in uracil,

$$I^- \cdot 2TU \xrightarrow{h\nu} I^- \cdot 2TU^* \rightarrow I^- \cdot 2TU \rightarrow I^- + 2TU. \qquad (7)$$
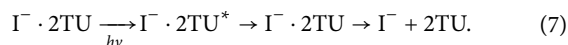
Ullrich and coworkers reported that the $\pi\pi^*$ (S_2) and $n\pi^*$ (S_1) states of the 2TU decay within 1 ps for excitation energies ranging from 4.25 to 4.98 eV.[43] Due to this rapid re-population of the ground state with considerable vibrational energy, the overall rate for iodide dissociation can still be determined by the statistical decay of the ground state. Although the calculated dissociation rates are near the limit where RRKM may fail owing to the incomplete intramolecular vibrational redistribution (IVR), the agreement between the calculated and experiment lifetimes at two excitation energies suggests that RRKM is an appropriate framework for the interpretation of our results.

The slower time constants for the decay of the VB states in 4.73 eV excitation are longer than 10 ps. Since this is longer than the timescale for iodide release, this slow decay does not contribute to the back electron transfer that leads to iodide dissociation. It is possible that these decays reflect disappearance of the VB state via deprotonation; we note that deprotonation of 2TU occurs via dissociative electron attachment at electron energies of 0.6 eV,[27] close to the difference between the 4.73 eV photon energy and the VDE of $I^- \cdot 2TU$. Moreover, the deprotonated anion cannot be photodetached at 3.18 eV.[38] Deprotonation is likely to be much less efficient at 4.16 eV excitation, so a portion of VB anions remains at relatively long time delays, giving rise to the offset component in the TRPE spectrum and to the low photofragmentation yields observed by mass spectroscopy.[24]

Feature D is a relatively weak signal that only appears with higher energy excitation. Previous computational work on 2TU tautomers with coupled cluster singles and doubles with perturbative triples correlations [CCSD(T)] have suggested that the tautomer R15, where a proton is transferred from N1 to C5, is more stable than the canonical form of 2TU and has a VDE of 1.66 eV.[29] This is almost identical to the eBE of feature D, which is centered around 1.7 eV, providing evidence for a tentative assignment of feature D as the tautomer.

C. Comparison with $I^- \cdot U$

In photoexcited $I^- \cdot U$, the measured rise times for fragmentation to I^- are 86 and 36 ps for near-VDE and 4.7 eV excitation, respectively. These values are noticeably slower than those found here for $I^- \cdot 2TU$, namely, 14 and 9 ps at the analogous excitation energies. The two rise times for $I^- \cdot 2TU$ are relatively consistent with RRKM values for the dissociation of vibrationally excited $I^- \cdot 2TU$, whereas those for $I^- \cdot U$ are considerably larger than the calculated RRKM values (8.6 and 4.4 ps). Hence, there appears to be a bottleneck to the formation of energized $I^- \cdot U$ that is absent in $I^- \cdot 2TU$.

For near VDE excitation of $I^- \cdot U$, the DB and VB states persist considerably longer than those seen here, with bi-exponential decay constants of 5 and 500 ps for the DB state and 5 and 80 ps for the VB state. Assuming that back electron transfer to the iodine is reflected in these decays, then this process, which is necessary for the formation of energized $I^- \cdot U$, is much slower than in $I^- \cdot 2TU$, and this may account for the slower iodide fragmentation channel in $I^- \cdot U$. As discussed above, the VB anion of $2TU^-$ lies below the DB anion, in contrast to canonical uracil, resulting in substantially more complete DB → VB conversion in photoexcited $I^- \cdot 2TU$. When only a small portion of the DB state can convert to the VB state, there may be a bottleneck for I^- production that decreases the rate at which transient states can decay. It seems likely that the rate of back electron transfer from the VB state is also key to understanding these dynamics, although further investigation will be necessary to elucidate all factors.

At the higher excitation energy, which is assigned primarily to $\pi\pi^*$ excitation in both $I^- \cdot U$ and $I^- \cdot 2TU$, internal conversion of the chromophore back to its ground electronic state will produce an energized complex that would be expected to undergo statistical decay, and this indeed appears to be the case in $I^- \cdot 2TU$. However, there is experimental and theoretical evidence that the bright S_2 $\pi\pi^*$ state in uracil relaxes to the dark S_1 $n\pi^*$ state where it can remain for many ps before reaching the ground state;[44,45] this process may be the dynamical bottleneck that results in the slower-than-statistical fragmentation to I^- + U. Ulrich and co-workers[43] found that the excited singlet states of 2TU relax within 1 ps, so the analogous bottleneck is not expected to play a role in the fragmentation of $I^- \cdot 2TU$. We note, however, that back-electron transfer from the VB anion is also expected to play a role in fragmentation to I^- at 4.73 eV excitation, so the overall mechanism for this process is complex and worthy of further investigation in both systems.

VI. CONCLUSIONS

TRPES with the combination of two different excitation (4.16 and 4.73 eV) and probe (1.59 and 3.18 eV) energies has been applied to $I^- \cdot 2TU$ clusters to observe the dynamics of low energy electron attachment to 2TU. The DB anion of 2TU is accessed immediately after near-VDE excitation and then decays to the VB state on a timescale of ~55 fs. It thus appears that the DB state of 2TU acts as a "doorway" to form the VB state. The energy gap between DB and VB states in 2TU is anticipated to be the driving force of this ultrafast internal process. We find that the interconversion from the DB to the VB anion is more complete in $I^- \cdot 2TU$ than in $I^- \cdot U$. This result is attributed to the VB anion of 2TU lying below its DB state, in contrast to U where the ordering is reversed. For 4.73 eV excitation, the DB feature is not observed, and in addition to the expected VB state, a higher-lying π^* anion forms before being rapidly (70 fs) deactivated.

At both excitation energies, we observe by means of a 3.18 eV probe pulse a strong feature that is clearly from dissociated I^-. The excitation energy-dependent dissociation dynamics are found to be in good agreement with those predicted by RRKM theory, suggesting that the vibrationally excited ground state $I^- \cdot 2TU$ is prepared without a dynamic bottleneck. Formation of the vibrationally excited $I^- \cdot 2TU$ is attributed to back electron transfer from the VB state at

both excitation energies and, at 4.73 eV, to $\pi\pi^*$ excitation followed by the internal conversion of 2TU to its ground state. The ~10 ps time scales for I$^-$ formation are in contrast to the much slower dissociation rates seen in previous TRPES experiments on I$^-$·U.

SUPPLEMENTARY MATERIAL

See the supplementary material for the details of RRKM calculation and curve fitting results in 4.16 eV excitation and 1.59 eV probe under the triple-exponential function.

AUTHOR DECLARATIONS

Conflict of Interest

The authors have no conflicts to disclose.

Author Contributions

Masafumi Koga: Conceptualization (equal); Data curation (lead); Formal analysis (lead); Funding acquisition (lead); Investigation (lead); Methodology (equal); Software (equal); Writing – original draft (equal); Writing – review & editing (equal). **Megan Asplund:** Conceptualization (equal); Data curation (equal); Formal analysis (equal); Investigation (equal); Software (equal); Writing – review & editing (supporting). **Daniel M. Neumark:** Conceptualization (lead); Methodology (equal); Project administration (lead); Resources (lead); Supervision (lead); Validation (lead); Writing – review & editing (equal).

DATA AVAILABILITY

The data that support the findings of this study are available from the corresponding author upon reasonable request.

REFERENCES

[1] B. Boudaïffa, P. Cloutier, D. Hunting, M. A. Huels, and L. Sanche, Science **287**, 1658–1660 (2000).

[2] P. D. Burrow, G. A. Gallup, A. M. Scheer, S. Denifl, S. Ptasinska, T. Märk, and P. Scheier, J. Chem. Phys. **124**(12), 124310 (2006).

[3] J. Gu, J. Leszczynski, and H. F. Schaefer, Chem. Rev. **112**(11), 5603–5640 (2012).

[4] J. N. Bull, C. W. West, and J. R. R. Verlet, Chem. Sci. **7**(8), 5352–5361 (2016).

[5] A. Kunin and D. M. Neumark, Phys. Chem. Chem. Phys. **21**(14), 7239–7255 (2019).

[6] S. B. King, M. A. Yandell, and D. M. Neumark, Faraday Discuss. **163**, 59–72 (2013).

[7] S. B. King, A. B. Stephansen, Y. Yokoi, M. A. Yandell, A. Kunin, T. Takayanagi, and D. M. Neumark, J. Chem. Phys. **143**(2), 024312 (2015).

[8] M. A. Yandell, S. B. King, and D. M. Neumark, J. Am. Chem. Soc. **135**(6), 2128–2131 (2013).

[9] A. B. Stephansen, S. B. King, Y. Yokoi, Y. Minoshima, W.-L. Li, A. Kunin, T. Takayanagi, and D. M. Neumark, J. Chem. Phys. **143**(10), 104308 (2015).

[10] S. B. King, M. A. Yandell, A. B. Stephansen, and D. M. Neumark, J. Chem. Phys. **141**(22), 224310 (2014).

[11] W.-L. Li, A. Kunin, E. Matthews, N. Yoshikawa, C. E. H. Dessent, and D. M. Neumark, J. Chem. Phys. **145**(4), 044319 (2016).

[12] A. Kunin, W.-L. Li, and D. M. Neumark, J. Chem. Phys. **149**(8), 084301 (2018).

[13] A. Kunin, V. S. McGraw, K. G. Lunny, and D. M. Neumark, J. Chem. Phys. **151**(15), 154304 (2019).

[14] A. Stolow, A. E. Bragg, and D. M. Neumark, Chem. Rev. **104**(4), 1719–1758 (2004).

[15] E. Matthews, R. Cercola, G. Mensa-Bonsu, D. M. Neumark, and C. E. H. Dessent, J. Chem. Phys. **148**(8), 084304 (2018).

[16] R. Cercola, E. Matthews, and C. E. H. Dessent, Mol. Phys. **117**, 3001–3010 (2019).

[17] R. Cercola, K. O. Uleanya, and C. E. H. Dessent, Mol. Phys. **118**(12), e1662128 (2020).

[18] J. H. Hendricks, S. A. Lyapustina, H. L. de Clercq, J. T. Snodgrass, and K. H. Bowen, J. Chem. Phys. **104**(19), 7788–7791 (1996).

[19] R. A. Bachorz, W. Klopper, and M. Gutowski, J. Chem. Phys. **126**(8), 085101 (2007).

[20] G. W. Anderson, I. F. Halverstadt, W. H. Miller, and R. O. Roblin, Jr., J. Am. Chem. Soc. **67**(12), 2197–2200 (1945).

[21] P. Ajitkumar and J. D. Cherayil, Microbiol. Rev. **52**(1), 103–113 (1988).

[22] M. Pollum, S. Jockusch, and C. E. Crespo-Hernández, J. Am. Chem. Soc. **136**(52), 17930–17933 (2014).

[23] J. Cohen, Science **372**(6549), 1381–1381 (2021).

[24] K. O. Uleanya and C. E. H. Dessent, Phys. Chem. Chem. Phys. **23**(2), 1021–1030 (2021).

[25] A. Khvorostov, L. Lapinski, H. Rostkowska, and M. J. Nowak, J. Phys. Chem. A **109**(34), 7700–7707 (2005).

[26] J. Kopyra, H. Abdoul-Carime, F. Kossoski, and M. T. d. N. Varella, Phys. Chem. Chem. Phys. **16**(45), 25054–25061 (2014).

[27] J. Kopyra, K. K. Kopyra, H. Abdoul-Carime, and D. Branowska, J. Chem. Phys. **148**(23), 234301 (2018).

[28] X. Li, J. Chen, and K. H. Bowen, J. Chem. Phys. **134**(7), 074304 (2011).

[29] O. Dolgounitcheva, V. G. Zakrzewski, and J. V. Ortiz, J. Chem. Phys. **134**(7), 074305 (2011).

[30] A. V. Davis, R. Wester, A. E. Bragg, and D. M. Neumark, J. Chem. Phys. **118**(3), 999–1002 (2003).

[31] A. E. Bragg, J. R. R. Verlet, A. Kammrath, O. Cheshnovsky, and D. M. Neumark, J. Am. Chem. Soc. **127**(43), 15283–15295 (2005).

[32] W. C. Wiley and I. H. McLaren, Rev. Sci. Instrum. **26**(12), 1150–1157 (1955).

[33] V. Dribinski, A. Ossadtchi, V. A. Mandelshtam, and H. Reisler, Rev. Sci. Instrum. **73**(7), 2634–2642 (2002).

[34] M. J. Frisch, G. W. Trucks, H. B. Schlegel, G. E. Scuseria, M. A. Robb, J. R. Cheeseman, G. Scalmani, V. Barone, G. A. Petersson, H. Nakatsuji, X. Li, M. Caricato, A. V. Marenich, J. Bloino, B. G. Janesko, R. Gomperts, B. Mennucci, H. P. Hratchian, J. V. Ortiz, A. F. Izmaylov, J. L. Sonnenberg, D. Williams-Young, F. Ding, F. Lipparini, F. Egidi, J. Goings, B. Peng, A. Petrone, T. Henderson, D. Ranasinghe, V. G. Zakrzewski, J. Gao, N. Rega, G. Zheng, W. Liang, M. Hada, M. Ehara, K. Toyota, R. Fukuda, J. Hasegawa, M. Ishida, T. Nakajima, Y. Honda, O. Kitao, H. Nakai, T. Vreven, K. Throssell, J. A. Montgomery, Jr., J. E. Peralta, F. Ogliaro, M. J. Bearpark, J. J. Heyd, E. N. Brothers, K. N. Kudin, V. N. Staroverov, T. A. Keith, R. Kobayashi, J. Normand, K. Raghavachari, A. P. Rendell, J. C. Burant, S. S. Iyengar, J. Tomasi, M. Cossi, J. M. Millam, M. Klene, C. Adamo, R. Cammi, J. W. Ochterski, R. L. Martin, K. Morokuma, O. Farkas, J. B. Foresman, and D. J. Fox, Gaussian 16, Rev. A.03, Gaussian, Inc., Wallingford, CT, 2016.

[35] K. A. Peterson, B. C. Shepler, D. Figgen, and H. Stoll, J. Phys. Chem. A **110**(51), 13877–13883 (2006).

[36] A. Kunin, W.-L. Li, and D. M. Neumark, Phys. Chem. Chem. Phys. **18**, 33226 (2016).

[37] M. A. Yandell, S. B. King, and D. M. Neumark, J. Chem. Phys. **140**(18), 184317 (2014).

[38] K. O. Uleanya, R. Cercola, M. Nikolova, E. Matthews, N. G. K. Wong, and C. E. H. Dessent, Molecules **25**(14), 3157 (2020).

[39] T. Baer, W. L. Hase, and L. William, *Unimolecular Reaction Dynamics: Theory and Experiments* (Oxford University Press on Demand, 1996).

[40] R. G. Gilbert and S. C. Smith, *Theory of Unimolecular and Recombination Reactions* (Publishers' Business Services, 1990).

[41] T. Beyer and D. F. Swinehart, Commun. ACM **16**(6), 379 (1973).

[42] S. E. Stein and B. S. Rabinovitch, J. Chem. Phys. **58**(6), 2438–2445 (1973).

[43] J. A. Sánchez-Rodríguez, A. Mohamadzade, S. Mai, B. Ashwood, M. Pollum, P. Marquetand, L. González, C. E. Crespo-Hernández, and S. Ullrich, Phys. Chem. Chem. Phys. **19**(30), 19756–19766 (2017).

[44] P. M. Hare, C. E. Crespo-Hernández, and B. Kohler, Proc. Natl. Acad. Sci. U. S. A. **104**(2), 435–440 (2007).

[45] S. Ullrich, T. Schultz, M. Z. Zgierski, and A. Stolow, Phys. Chem. Chem. Phys. **6**, 2796–2801 (2004).